Three-body constrained bosons in Su-Schrieffer-Heeger(SSH) type model: Quantum phases, edge states and topological charge pumping

Suman Mondal[1], Sebastian Greschner[2] and Tapan Mishra[1]

[1]*Department of Physics, Indian Institute of Technology, Guwahati-781039, India and*

[2] *Department of Quantum Matter Physics, University of Geneva, 1211 Geneva, Switzerland*

(Dated: December 20, 2018)

We analyse the ground-state properties of three-body constrained bosons in a one dimensional optical lattice with staggered hopping analogous to the well known Su-Schrieffer-Heeger(SSH) model. By considering attractive and repulsive on-site interactions between the bosons, we obtain the phase diagram which exhibits various quantum phases. Due to the double-well geometry and three-body constraint several gapped phases such as the Mott insulators and dimer/bond-order phases emerge at commensurate densities in the repulsive interaction regime. Attractive interaction leads to the pair formation which leads to the pair bond order phase at unit filling which resembles the valence-bond solid phase of composite bosonic pairs. The pair bond order phase at unit-filling is found to exhibit effective topological properties due to the lattice structure, such as the presence of polarized paired edge states. Finally we study the emergence and breakdown of Thouless charge pumping of bosonic pairs in the bond order phase.

I. INTRODUCTION

Ultracold atoms in optical lattices with tunable interactions and lattice parameters have opened up a wide area of research in recent years. The significant progress both in theoretical and experimental fronts have uncovered a wealth of new physics which was impossible to achieve in the conventional solid state systems. The path breaking observation of the superfluid (SF) to Mott insulator (MI) transition [1] following its theoretical prediction [2] in a system of ultracold bosons in optical lattice have paved the path to simulate complex quantum many-body physics [3]. The exquisite control over the interactions and lattice geometries are the key to achieve such interesting physics. A new frontier of research have evolved with the construction of superlattices which is an array of double-well potentials [1, 4–9]. Recent experiments on systems of ultracold atoms in these double wells have led to various interesting phenomena ranging from condensed matter physics, atom interferometry to quantum information. Particularly in one dimension these double-well lattices exhibits interesting properties due to the staggered or dimerized hopping amplitudes. The presence of this staggered hopping resembles these system to the inversion symmetric Su-Schrieffer-Heeger(SSH) model for fermions [10] which possess interesting topological features given by the Zak phase. The SSH model has been widely explored theoretically [11–13] and also in recent experiments [14, 15]. It is important to note that the bosonic analogue of such model also provides insights about the topological phase transitions of the gapped phases at half-integer densities which are protected by the inversion symmetry of the Hamiltonian [16]. These topological phases are characterised by the existence of the edge states. Another interesting feature of these topological phase transition is the Thouless charge pumping which has attracted a great deal of attention recently [17–21].

On the other hand the experimental observation of

local higher order interactions in optical lattices have opened up a new direction to simulate quantum phase transition in the presence of multi-body interaction [22]. Several interesting ideas have been proposed to engineer and tune such interactions in optical lattices [23–27]. One of such example is the possibility to create a situation where the three-body interaction can become extremely large. Under this circumstance the bosons will experience three-body hardcore constraint [28], which prohibits more than two atoms to occupy a single lattice site. This condition facilitates to explore the physics of attractive Bose-Hubbard model which otherwise leads to collapse of atoms onto a single site. Many novel scenarios have been investigated recently by considering three-body constrained bosons in optical lattices [28–34]. The physics which is manifested by the two body interaction along with the large three body repulsion is one of the simplest problem to understand although it has interesting physical implications. In such a scenario the system exhibits the usual SF-MI phase transition for repulsive on-site interaction and for attractive interactions there exists a superfluid to pair superfluid (PSF) phase transition [29].

In the case of attractive interaction in particular, the interplay between pair formation and formation of topo-
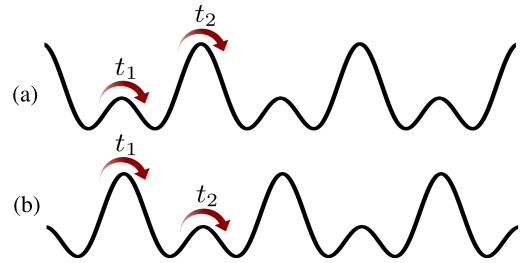

FIG. 1: One dimensional double well optical superlattice with staggered hopping (a) $t_1 > t_2$ and (b) $t_1 < t_2$.

logical edge states may lead to interesting physics. Recently, in the framework of two-body calculations, Di Liberto et al. in Refs. [35] explored the formation of edge states of (repulsively) bound pairs beyond standard bulk-boundary correspondence. The paradigm of the three-body constrained bosons may allow to extend these ideas to a many-body context. In particular at a commensurate unit-filling as we will show in the following one observes the presence of unconventional edge states and topological charge pumping of composite bosonic pairs.

In this paper we consider a system of three-body constrained bosons in a double well optical superlattice in one dimension i.e. the bosonic SSH type model as shown in Fig. 1(a). The presence of double well potentials creates a situation with staggered hopping amplitudes. This superlattice geometry can be created by superimposing two lattices with one lattice having double the period of the other. One may notice that this system can have two different types of geometries by interchanging the hopping amplitudes as shown in Fig. 1(b).

The physics of ultracold bosons in double well optical lattice can be explained by a modified Bose-Hubbard model with staggered hopping amplitudes(bosonic SSH model) which is given as;

$$\mathcal{H} = -t_1 \sum_{i \,\in\, odd} (a_i^\dagger a_{i+1} + \text{H.c.})$$
$$- t_2 \sum_{i \,\in\, even} (a_i^\dagger a_{i+1} + \text{H.c.}) + \frac{U}{2} \sum_i n_i(n_i - 1) \quad (1)$$

where $a_i^\dagger$ and a_i are the creation and annihilation operators for bosons at site i and $n_i = a_i^\dagger a_i$ is the number operator at site i. t_1 and t_2 are the tunneling rates from odd and even sites respectively. The onsite contact interactions are characterized by the term U. The bosons in the lattice enjoy three-body constraint i.e. $(a_i^\dagger)^3 = 0$. Based on the arrangements of the hopping strengths, there exists two types of situation i.e. with $t_1 > t_2$ (Fig. 1(a)) and $t_1 < t_2$(Fig. 1(b)).

It is important to note that both types of dimerization exhibit identical bulk properties. At half filling the single particle spectrum is gapped for any imbalance in hopping between the unit cells $t_1 \neq t_2$ [10]. The ground state is a dimer phase or bond order(BO) phase for spin polarized fermions or bosons with very large on-site interactions (hardcore bosons). Due to the chiral symmetry of the model in this case, for $t_1 < t_2$ gapless topological edge state emerges characterized by a nontrivial winding number (or Zak phase) [36–38]. This condition however, will be different in the case of three-body constrained bosons which we analyse in the present work. We analyse the ground state properties both for repulsive and attractive on-site interactions obtaining the complete phase diagram as discussed below. We first discuss the bulk physics by considering $t_1 > t_2$ and in the end we will consider the case of $t_1 < t_2$.

We assume $t_1 = 1$ (unless stated otherwise) which makes other physical quantities dimensionless. Ground
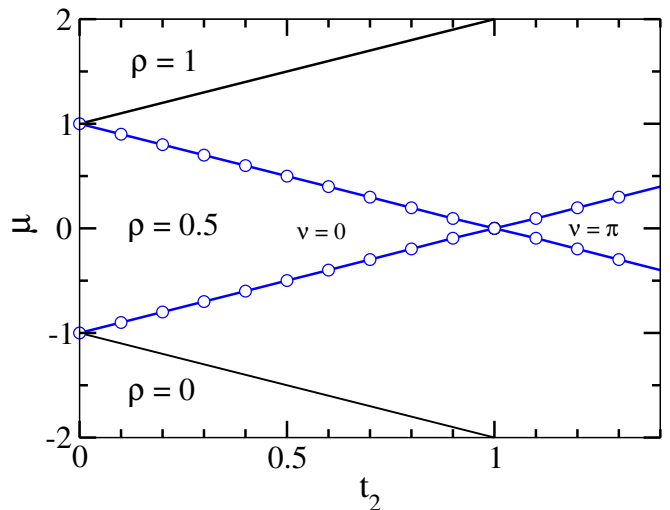

FIG. 2: (Color online)Phase diagram of hardcore bosons with $t_2 = 0.2$. The region included by the blue circles is the bond-ordered (BO) phase at half filling. The black curves represent the empty and full states.

state properties of this system is analysed using the density matrix renormalization group (DMRG) method. We consider system sizes up to 160 sites and retaining up to 800 density matrix eigenstates.

The rest of the paper is arranged as follows. In Sec. II we discuss the limiting focusing on hardcore bosons in SSH type model and the physics in the limit of isolated double wells. In Sec. III, we present the general phase diagram with different values of twobody onsite interactions. Section IV is devoted to the analysis of the gapped phases at unit filling. In Section V we discuss in detail the emergence of edge states in this regime and extend the discussion topological charge-pumping in the related Rice-Mele [39] model and conclude in Sec. VI.

II. LIMITING CASES

We begin our discussion with a short summary of the properties of two analytical solvable limits of model (1).

A. $U = \infty$ limit

In the limit of large interactions $U \to \infty$, the bosons are hardcore in nature and in this limit the Model (1), after a Jordan-Wigner transformation to free fermions, can be considered as the topological SSH model as mentioned before. Due to the staggered hopping amplitudes, the SSH model at half filling dimerizes naturally due to the Peierls instability and one gets dimerized phase of bosons. In this phase a single boson lives in one of the unit cell composed of two lattice sites in the double-well with larger hopping strength. Doping away from half filling breaks this dimer ordering and a critical SF phase
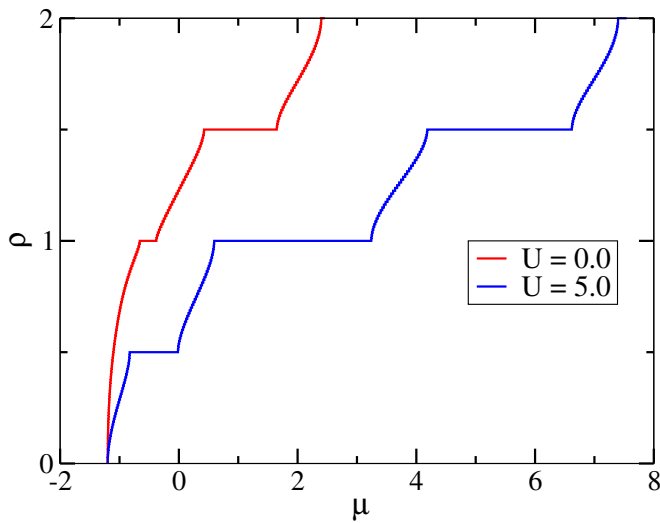
FIG. 3: (Color online)Figure shows the behaviour of ρ with respect to μ for $U = 0$ (left red curve) and $U = 5$ (right blue curve) for $t_2 = 0.2$. Plateaus indicate the gapped phases.

appears. This gapped phase is called the BO phase. The phase diagram of such system is shown in Fig. 2 as a function of t_2 and the filling. The gapped phases are characterized by the finite single particle gaps which is defined as

$$E_G = \mu^+ - \mu^-, \qquad (2)$$

where μ^+ and μ^- are the chemical potentials. As it can be seen from the phase diagram, any finite hopping imbalance leads to the gapped phase which is a bond-ordered (BO) phase and this phenomenon is also evident from the single particle spectrum. As discussed in Refs. [16], the gapped regions for $t_2 < t_1$ and $t_2 > t_1$ may be discriminated by the presence of gapless edge states in the latter case and a non-vanishing topological winding number $\nu = \pi$, which for the free fermion wave-functions ψ_k at lattice-momentum k is given by

$$\nu = \int_0^{2\pi} dk \langle \psi_k | \partial_k | \psi_k \rangle \qquad (3)$$

and as shown in Fig. 2. This paradigmatic example of bulk-boundary-correspondence can be extended to the case of softcore bosons [16] and we will explore its validity for composite bosonic pairs in Section (IV).

B. Isolated Double Wells

It is also instructive to discuss of the model from the case of trivially disconnected double-wells, corresponding to the case $t_2 = 0$. The model Hamiltonian is readily diagonalized for a fixed particle number: In the $\rho = 1$ ($\rho = 3$) sector two eigen-energies $\pm t_1$ ($U \pm 2t_1$) are found. For $\rho = 2$, the eigenvalues are given by U

and $\frac{1}{2}\left(U \pm \sqrt{16t_1^2 + U^2}\right)$. With these eigenvalues in a grand-canonical ensemble three gapped phases at fillings $\rho = 0.5$, 1 and 1.5 can be be observed (see inset of Fig. 5) in the strong dimerization limit. In this limit the gap at unit filling is given by $\Delta_{\text{gap}} = -3t_1 + \sqrt{16t_1^2 + U^2}$.

The ground state in the $n = 1$ sector is given by $|\psi_1\rangle = \psi_{20}|2,0\rangle + \psi_{11}|1,1\rangle + \psi_{02}|0,2\rangle$. Here $|n_1, n_2\rangle$ denotes a Fock-state basis of the isolated double well and $\psi_{02} = \psi_{20} = 2/\sqrt{16t_1^2 + 2U\varepsilon}$, $\psi_{11} = 2\varepsilon/\sqrt{16t_1^2 + 2U\varepsilon}$ where $\varepsilon = U/2 + \sqrt{4t_1^2 + U^2/4}$. For $U \to \infty$ this results in a MI like state $\sim |11\rangle$ and a dimer of pairs $|20\rangle + |02\rangle$ (pair-bond-ordered or PBO phase) for strong attractive interactions with a smooth crossover between both regimes. Indeed, the decoupled double well ground state for $U = 0$ resembles a superposition of MI and PBO states. The features of this interesting many-body state for finite hopping $t_1, t_2 \neq 0$ will be studied in Sections (III) and (IV).

A finite small hopping $0 < t_2 \ll 1$ will couple the double wells and allow for a melting of the gapped phases due to the energy gain by delocalization of excitations and stabilize superfluids separating the gapped phases. This process may be understood as well from a effective model of coupled dimer-states such as recently discussed in Refs. [35].

For open boundary conditions the case $t_1/t_2 = 0$ reveals the topological nature of the SSH model, details will be discussed in section V.
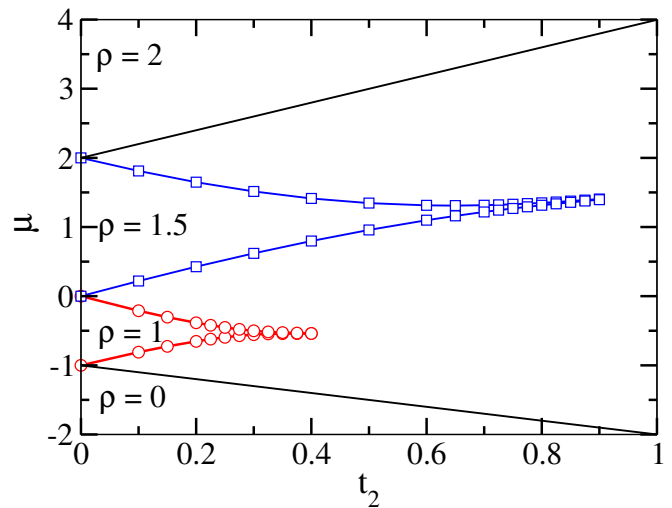

FIG. 4: (Color online)The phase diagram for three-body constrained bosons as a function of t_2 for $U = 0$ obtained from polynomial extrapolation of gap. The BO phase at $\rho = 1$ and $\rho = 1.5$ appear at $t_2 \sim 0.4$ and $t_2 \sim 0.9$ respectively.

III. GENERAL PHASE DIAGRAM

A. Vanishing two-body interaction($U = 0$)

In the limit of vanishing interactions for a softcore boson without the three-body hardcore constraint one expects an SF phase even for very strong hopping imbalance. In the presence of interaction the physics of the system is governed by the competition between the hopping amplitudes and the onsite interactions which leads to the non-trivial gapped phases at intermediate half integer filling apart from the gapped MI phases [16] as a function of interaction U. A similar feature is also present in the case of usual two color superlattice potential where the SF phase becomes gapped MI phases at half integer and integer fillings for strong interactions [40].

The situation however, is different in the case of three-body constrained bosons where a maximum of two bosons can occupy a single lattice site. Due to the effect of double well superlattice the motion of particles is restricted to one unit cell. Interestingly, in such a scenario two different gapped phases arise at $\rho = 1$ and $\rho = 1.5$ after some critical values of t_2. The gap in the system can be seen as the finite plateaus in the ρ vs μ diagram as shown in Fig. 3. The phase diagram corresponding to this scenario is depicted in Fig. 4 where the gapped phases at $\rho = 1$ and $\rho = 1.5$ appear at $t_2 \sim 0.4$ and $t_2 \sim 0.9$ respectively. The gapped BO regions for $\rho = 1$ and $\rho = 1.5$ are bounded by red circles and blue squares respectively. The black lines correspond to the empty and full states. The remaining part of the phase diagram is the SF phase.

B. $t_2 = 0.2$ case

As the system is already in the gapped BO phase for $U = 0$ at commensurate densities except at $\rho = 0.5$, it is interesting to see the effect of interactions on the ground state of the system. The phase diagram for this case is shown in Fig. 5. As we move away from the $U = 0$ limit along the positive U axis the gapped phases grow as can be seen from the enlargement of the plateaus in the ρ vs μ plot for $U = 5$ shown in Fig. 3. The gapped phases at $\rho = 0.5$ and $\rho = 1.5$ are depicted by the region bounded by the blue dashed curves and the one at $\rho = 1$ is bounded by the green solid curve in the phase diagram of Fig. 5. At $\rho = 0.5$, the gap appears after a critical point $U \gtrsim 0.4$ leading to the BO phase. As anticipated in the discussion of the decoupled double-well case, the excitation gap at $\rho = 1$ remains finite for all U even for a small $t_2 > 0$ leading to a smooth cross-over from the pair-bond-ordered (PBO) phase to the MI phase through the BO phase where every site is occupied by one atom due to large onsite repulsion. The strong onsite repulsion disfavours the dimerization and prohibits two particles occupying a single site. We will discuss this case in Section (IV) in more detail. For $\rho = 1.5$, the system remains in the BO phase which becomes wider as a function of
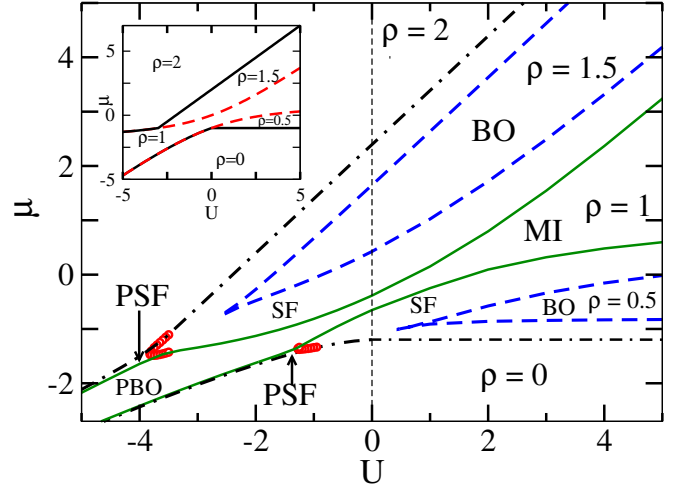

FIG. 5: (Color online)Phase diagrams for $t_2 = 0.2$. The region bounded by the green curves are the gapped phases at $\rho = 1$(middle) which consists of the MI(PBO) phases in the strong repulsive(attractive) regimes. The regions bounded by the blue dashed curves are the gapped BO phases at $\rho = 0.5$(upper) and $\rho = 1.5$(lower). On the attractive side the PSF is separated from the SF phase by the red circles. Inset shows the phase diagram in the limit of isolated double-wells.

U. This BO phase is similar to the one for the hardcore bosons at $\rho = 0.5$ as discussed before. The boundaries for the gapped phases are obtained by computing the chemical potentials μ^+ and μ^- and extrapolating them to thermodynamic limit using system sizes of $L = 20$, 40 and 80.

The signature of the BO phases are obtained by computing the bond-bond correlation function and the related structure factor which is given as;

$$S_{BO}(k) = \frac{1}{L^2} \sum_{i,j} e^{ikr} \langle B_i B_j \rangle, \qquad (4)$$

where $B_i = (a_i^\dagger a_{i+1} + H.c)$ is the bond operator. In the BO phase the quantity B_i oscillates in alternate bonds and the structure factor exhibits a finite peak at the zone boundaries. It is to be noted that the BO phases which appear in the phase diagram are not the true BO phase as lattice translational symmetry is not spontaneously broken. However, the signature is similar to the BO phase whose qualitative feature can be seen from the bond order structure factor.

The situation becomes interesting in the attractive regime. Because of the three-body constraint the system is stable against collapse and due to the attractive interaction, the particles start to form pairs. While there is no gapped phase at $\rho = 0.5$ in this side of the phase diagram, the gap at $\rho = 1.5$ remains finite up to some finite values of U and then closes after a critical point of $U = -2.6$. The closing up of the gap is due to the competition between the hopping and attractive interaction which tries to break the dimerization and system
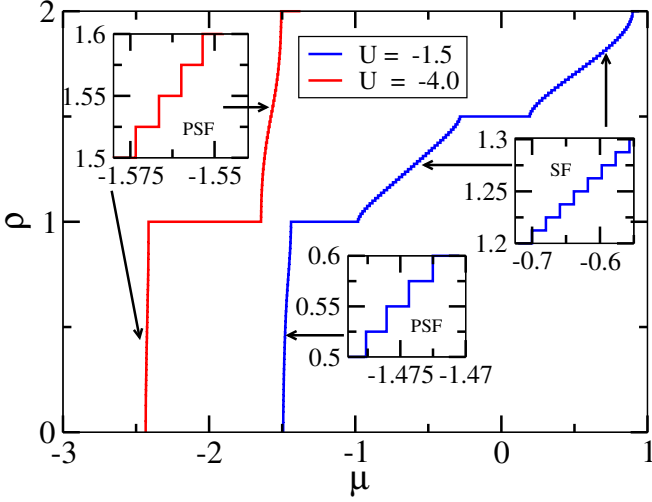
FIG. 6: (Color online)Behaviour of ρ with respect to μ for $U = -4.0$ (left red curve) and $U = -1.5$ (right blue curve) at $t_2 = 0.2$. The insets shows the enlarged regions of the SF and PSF phases where the density jumps in steps of one and two particles respectively.
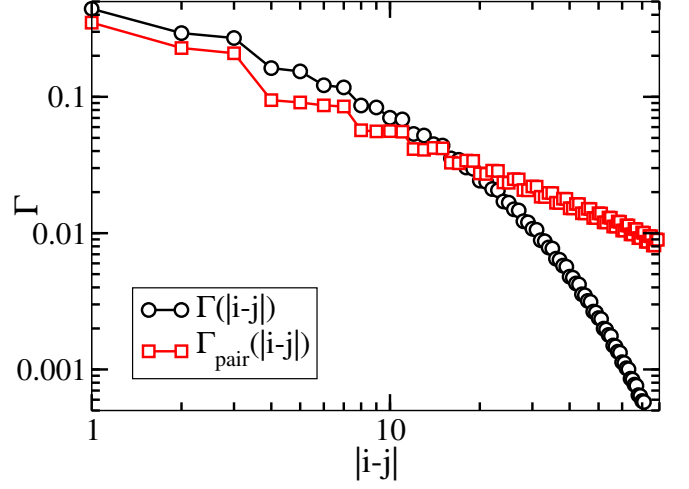

FIG. 7: (Color online)Single particle correlation function $\Gamma(|i-j|)$ (black circles) and pair correlation functions($\Gamma(|i-j|)$ for $t_2 = 0.2$ are plotted for $U = -4.0$ at $\rho = 1.5$ for a system of length $L = 160$ (see text for details).

becomes a superfluid as shown in the Fig. 5. However, for $\rho = 1$, the gap survives for very large values of U extending up to infinity. These features can be seen from the plateaus in the $\rho - \mu$ plot as shown in Fig. 6 for two different values of $U = -1.5$ and $U = -4.0$. For $U = -1.5$, the gaps appear at $\rho = 1$ as well as at $\rho = 1.5$ where as for $U = -4$, only the gap at $\rho = 1$ exists. For sufficiently strong attractive interaction, the particles tend to form pairs and at unit filling it becomes a half filled system of bosonic pairs. It is to be noted that these pairs behave like hardcore bosons due to the three-body constraint. In such a scenario the ground state is similar to the dimerization of the hardcore bosons as discussed in the section for $U = \infty$ case. The gapped phase for large attractive U is the BO phase of pairs which can be called as a PBO phase. However, in the weak interaction regime pair formation is not favoured due to the competition between the interaction and kinetic energy. Therefore, the BO phase which appear at $U = 0$ survives up to a finite value of attractive U and then there exist a smooth crossover to the PBO phase as the value of U increases.

The gapped BO phase which continues from the repulsive side for $\rho = 1.5$ closes at a critical value $U \sim -2.6$. It is interesting to note that as the interaction becomes more and more attractive, the pair formation occurs and a PSF phase is stabilized for all densities around $\rho = 1.0$ [29, 32]. The PSF and SF phases are separated by the red circles as depicted in the phase diagram of Fig. 5. The signature of PSF phase can be obtained from the $\rho - \mu$ plot where the density jumps in steps of two particle at a time to minimize the energy. This is clearly visible in the insets of Fig. 6 where the densities for two different values of U are plotted. For $U = -1.5$, the sys-

tem is in a PSF phase in the region below the $\rho = 1$ gapped phase and rest of the region is in the SF phase for incommensurate densities. However, for $U = -4$ the system is in the PSF phase for all values of density except $\rho = 1$. Apart from the $\rho - \mu$ curve, we compute the single particle and pair correlation functions and corresponding momentum distribution to confirm the existence of the PSF phase. Fig. 7 shows the behaviour of $\Gamma(i, j)$(black circles) and $\Gamma_{pair}(i, j)$(red squares) with respect to the distance $|i - j|$ for $U = -4$ and $\rho = 1.5$. It can be clearly seen that the single particle correlation function decays faster where as the pair correlation function behaves like
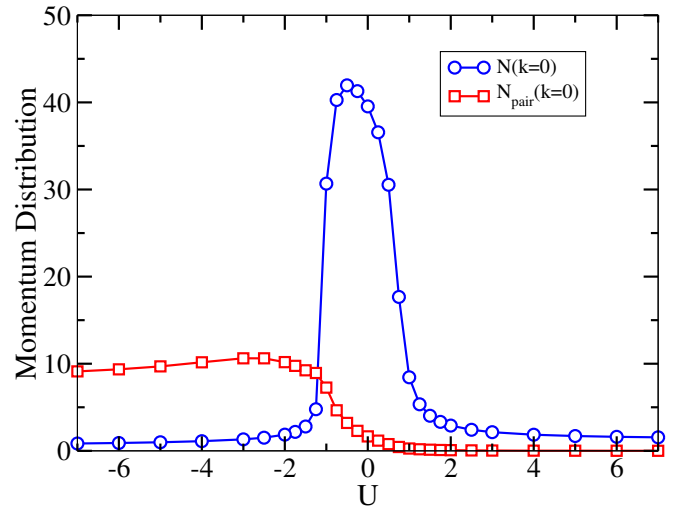

FIG. 8: (Color online)The peak heights of $N(k = 0)$ (blue circles) and $N_{pair}(k = 0)$ (red squares) at $\rho = 0.5$ using $L = 160$ show the transition from PSF to SF and then to BO phases as discussed in the text.
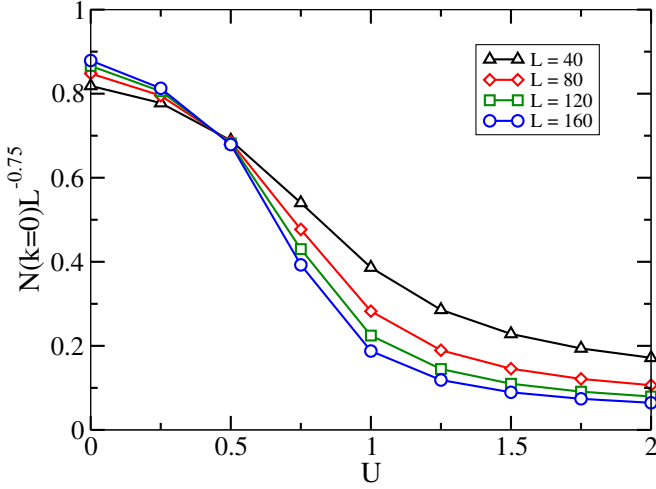
FIG. 9: (Color online)Finite size scaling of $N(k = 0)$ for $t_2 = 0.2$ shows that the curves for different lengths ($L = 40, 80, 120, 160$) intersect at the critical point $U \sim 0.44$ for the SF-MI transition at $\rho = 0.5$.

a power-law in the logarithmic scale which indicates the presence of the PSF phase.

We also compute the momentum distribution function

$$N(k) = \frac{1}{L} \sum_{i,j} e^{ikr} \Gamma(i,j), \qquad (5)$$

to complement the SF phases. Where $\Gamma(i,j) = \langle a_i^\dagger a_j \rangle (\langle a_i^{\dagger 2} a_j^2 \rangle)$ is the single particle(pair) correlation function. In Eq. 4 and Eq. 5 $r = |i - j|$ represent the distance between the lattice sites. The peak heights of the momentum distribution function $N(k = 0)$ for single particle and pairs are plotted against U in Fig. 8 for a cut through the phase diagram of Fig. 5 which corresponds to $\rho = 0.5$. This shows that for large attractive interaction $N_{pair}(k = 0)$ is dominant indicating the PSF phase. As the value of U becomes less attractive then the value of $N_{pair}(k = 0)$ decreases and $N(k = 0)$ increases showing the signatures of the SF phase. The SF phase continues till the critical point for SF-BO transition on the repulsive side where both the momentum distribution functions are extremely small.

The SF-BO transitions are of Berezinskii-Kosterlitz-Thouless(BKT) type transition which can be seen from the smooth opening up of the gap in Fig. 5. The transition points can be accurately obtained by performing a finite size scaling of the single particle momentum distribution function which varies as $N(k = 0) \propto L^{1-\frac{1}{2K}}$ [41], where $K = 2$ is the Luttinger parameter. In Fig. 9 we plot $N(k = 0)L^{-3/4}$ for different lengths($L = 80, 120, 160$) and all the curves intersect at the critical point $U \sim 0.44$.
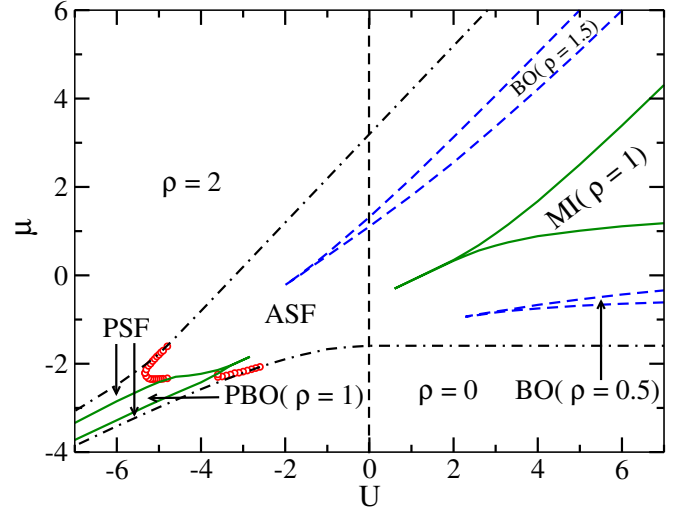

FIG. 10: (Color online)Phase diagrams for $t_2 = 0.6$. The region bounded by the continuous green curves are the gapped phases at $\rho = 1$ and the regions bounded by the blue dashed curves are the gapped bond order phases at $\rho = 0.5$ (upper) and 1.5 (lower). On the negative U side the PSF is separated from the SF phase by the red circles. The black dot-dashed lines represent the empty and full states.

C. $t_2 = 0.6$ case

After analyzing the phase diagram for the $t_2 = 0.2$ case where the effect of staggered hopping is large, we repeat the calculation for another cut through the phase diagram of Fig. 4 at $t_2 = 0.6$. The motivation to consider $t_2 = 0.6$ lies in the fact that there is no gap at $\rho = 1$ for $U = 0$ as depicted in Fig. 4 and it will be interesting to see how the system evolves by moving away from the
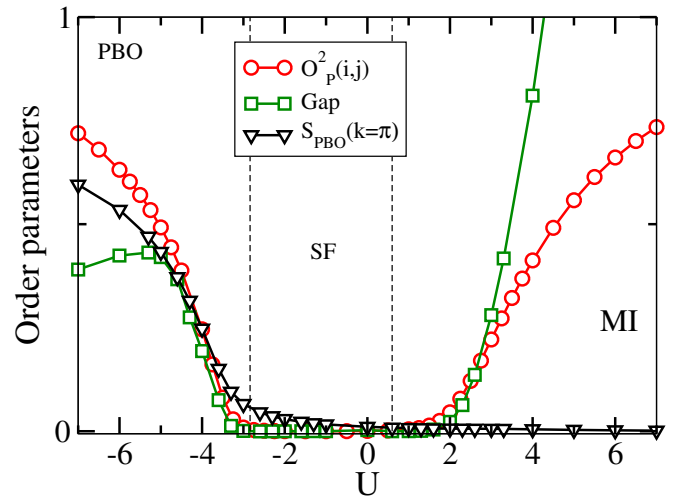

FIG. 11: (Color online)Order parameters depicting different phases for $t_2 = 0.6$. The red circles, green squares and black down triangles show the values of $O_P^2(i, j)$, $E_G(L)$ and $S_{PBO}(k = \pi)$ respectively for different values of U.
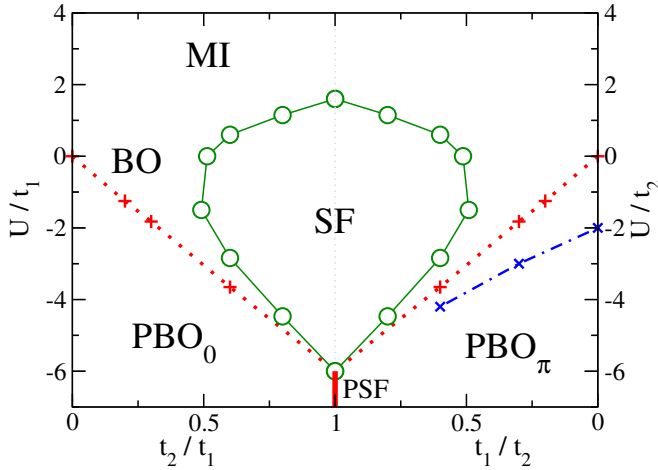
FIG. 12: (Color online)Phase diagram of the bosonic 3-body constraint SSH model at unit filling $n = 1$ as function of t_2/t_1 and U/t_1 (on the left) and t_1/t_2 and U/t_2 (right part). The straight lines mark BKT phase transitions between gapped and gapless phases. The dotted line depicts the crossing between single and two particle excitations and defines the crossover between MI and PBO phases. The dash-dotted line depicts the emergence of polarized edge states due to the non-trivial effective topology of the model in the attractive regime (see text).

non-interacting limit when the system is gapless. A similar analysis along the line of $t_2 = 0.2$ case leads to the phase diagram as shown in Fig. 10. It can be seen that the overall picture of the phase diagram is similar to that of $t_2 = 0.2$ for $\rho = 0.5$ and $\rho = 1.5$. However, interesting thing to note that there are clear phase transitions from the SF phase to the MI phase on the repulsive side of U and to a PBO phase on the attractive side of U. This signatures can be clearly seen from various order parameters plotted in Fig. 11 which will be discussed in detail in the following sections.

IV. GAPPED PHASES AT UNIT FILLING

In this section we provide a thorough analysis of the gapped phases at unit filling $\rho = 1$ which exhibit the interesting crossover between different gapped phases. In Fig.12 we show the phase diagram for unit filling $\rho = 1$ as function of the hopping ratios t_2/t_1 as well as t_1/t_2 and the interaction strength U/t_1 and U/t_2 respectively.

A. PBO-BO-MI crossover

The characteristic feature of the PBO phase is seen from the PBO structure factor $S_{PBO}(k)$ which is similar to the BO structure factor as defined in Eq. (4) with $a^\dagger(a)$ replaced by $a^{\dagger 2}(a^2)$ which is shown in Fig. 13. It can be seen that the value of $S_{PBO}(k = \pi)$ increases smoothly as
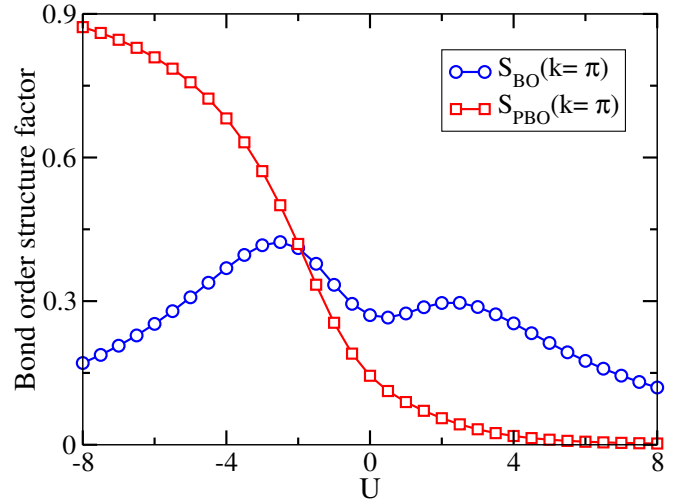

FIG. 13: (Color online)The extrapolated values of bond order structure factor for single particle (blue circles) and pairs (red squares) for different values of U at $\rho = 1$ (see text for details).

the value of U becomes more and more attractive. At the same time the BO structure factor $S_{BO}(k = \pi)$ decreases smoothly after increasing up to a particular value of attractive interaction $U \sim -2.5$. Note that the finite value of $S_{PBO}(k = \pi)$ for repulsive U and small attractive U are due to the finite probability of second order hopping processes in the BO phase. We would like to stress that since the BO phases are the manifestation of the double well geometry of the lattice, the BO structure factor is finite even in the the MI and PBO phase even in the thermodynamic limit. It can be seen from Fig. 13 that on the repulsive interaction side the value of $S_{BO}(\pi)$ smoothly decreases after a particular value of U. This signals the crossover to the MI phase. The onset of the MI phase can be understood as in the case of large interaction U, the system prefers to accommodate one particle in each site which is also true in the homogeneous lattice systems. This can be seen from the decreasing trend of the curve shown in the Fig. 13. We may further quantify the crossover point from the MI/BO region to the PBO phase by an analysis of the excitation gap. As shown in Fig. 14 we observe a crossing between the single particle gap $E_{G,1}$ and two-particle gap $E_{G,2}$ with

$$E_{G,m}(L) = \frac{E_0(N + m, L) - 2E_0(N, L) + E_0(N - m, L)}{m},$$

where $E_0(N, L)$ is the ground-state energy of a system of N particles and L sites and $m \in [1, 2]$. In the figure we show the data for $L = 80$ (dotted curve) and $L = 160$ (dashed curve) along with the extrapolated data (solid curve) for $t_2 = 0.6$. The extrapolation is performed using the data for $L = 40, 80, 120, 160$. This line defines the crossover between MI-like and dimerized PBO states. The crossover position to a PBO region shown already before which is depicted by the red cross-dotted line in

Fig. 12 an approximately corresponds to the crossing of $S_{PBO}(k)$ and $S_{BO}(k)$ curves such as in Fig. 13.

We may further characterize the position of the phase cross-over by local maximum of the fidelity susceptibility [42] (see Fig. 15)

$$\chi_{FS}(U) = \lim_{U-U'\to 0} \frac{-2\ln|\langle\Psi_0(U)|\Psi_0(U')\rangle|}{(U-U')^2}, \quad (7)$$

with the ground-state wave function $|\Psi_0\rangle$. While phase transitions are often characterized by a peak diverging with the system size length L, here we observe a stable maximum as function of several system sizes.

B. SF phase transition

The MI-SF phase transition is of BKT type. We estimate the transition points by means of the momentum scaling method described above. In order to verify the BKT character of the phase transitions in the attractive side we analyse the finite size scaling of the energy gaps using the approach used in Ref.([43, 44]). In the inset of Fig. 14 the rescaled single particle energy gap $\Delta_1' = \Delta_1 L(1 + 1/(\log(L) + C))$ for $t_2 = 0.6$ exhibits the expected scaling close to the BKT transition point($U_c = -2.9$) leading to a collapse of data points plotted against $x_L = \log L - \log B/\sqrt{|U-U_c|}$, with fitting parameters C, B and U_c [43, 44]). The SF-MI transition is depicted by green circles in Fig. 12.
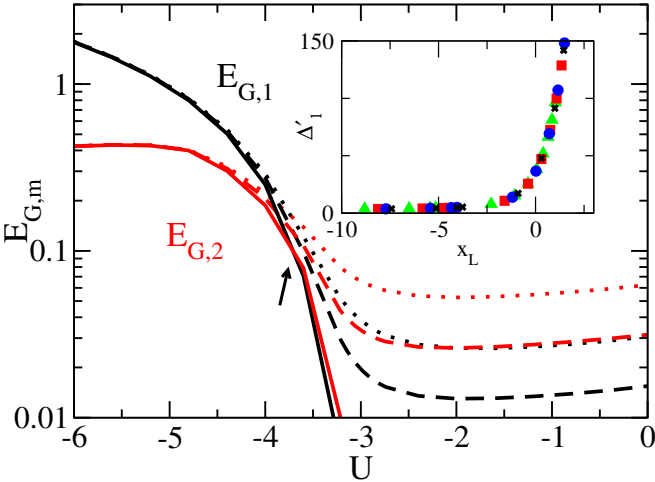

FIG. 14: (Color online)Single and two particle energy gap $E_{G,1}$ and $E_{G,2}$ for several system sizes $L = 80$ (dotted lines) and $L = 160$ (dashed line) together with the extrapolation to the thermodynamic limit (solid line, from $L = 40, 80, 120$ and 160 sites). DMRG data for $t_2/t_1 = 0.6$. The arrow marks the crossing between $E_{G,1}$ and $E_{G,2}$. The Inset shows the BKT-compatible scaling of the single particle energy gap with a critical value of $U_c = -2.9t_1$ (see text).
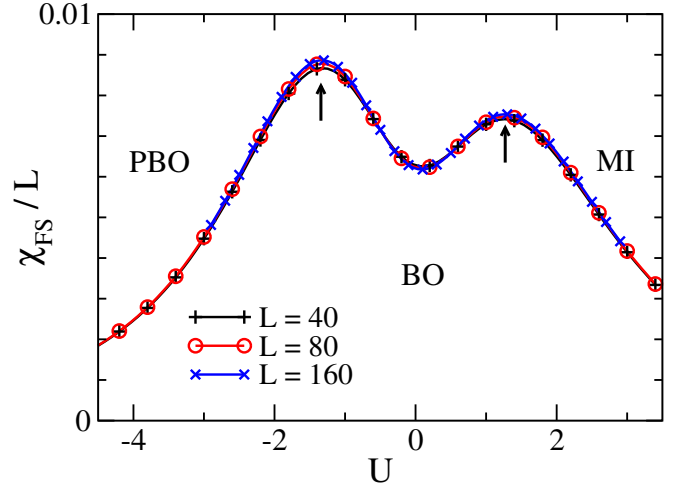

FIG. 15: (Color online)Fidelity susceptibility χ_{FS} as function of the interaction strength U ($n = 1$, $t2 = 0.2$) for $L = 40, 80$ and 160.

C. Parity order

Another physical quantity of interest which can be directly accessed in the state-of-the art experiment [45, 46] is the parity order parameter which is defined as

$$O_P^2(i,j) = \langle e^{i\sum_{i<k<j}\pi n_k}\rangle \quad (8)$$

To complement our findings we compute $O_P^2(i,j)$ which is finite in the MI phase due to particle-hole excitations. For small $t_2 \to 0$ we may understand the emergence of parity order from the properties of isolated double wells as discussed in Sec. II B. For a ground-state at $\rho = 1$ given by a product of $|\psi_1\rangle$, one easily estimates the parity order to be exactly $O_{P,e} = 1$ on even distances $|i-j|$. For
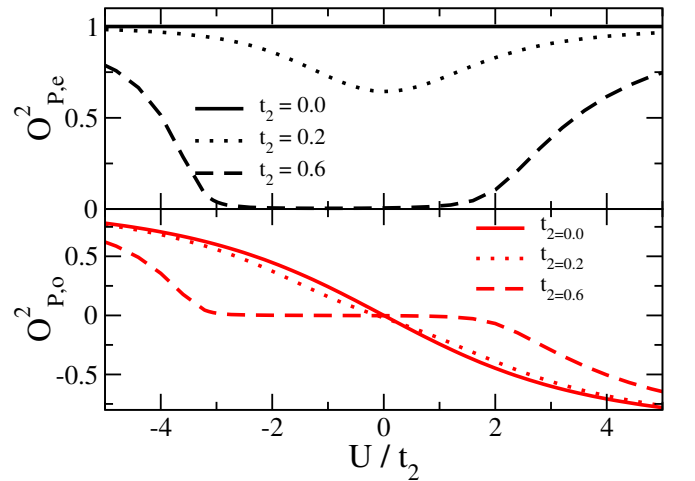

FIG. 16: (Color online)Parity order $O_P^2(i,j)$ for odd and even distances $|i-j| \gg 1$. $t_2 = 0$ lines correspond to the analytical results as discussed in the main text, $t_2 = 0.2$ and $t_2 = 0.6$ curves depict the data obtained for $L = 160$ sites.
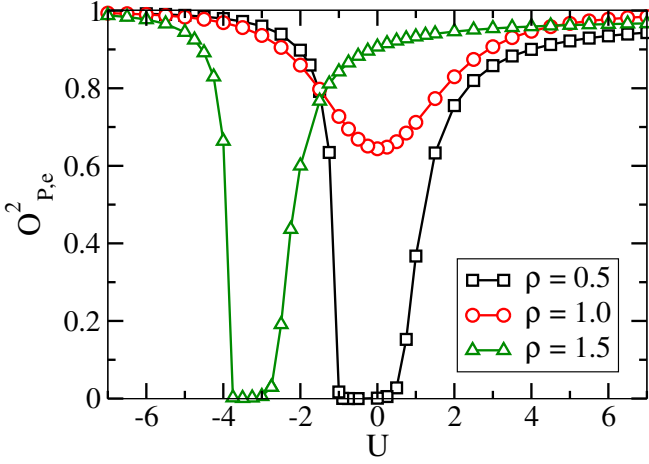
FIG. 17: (Color online)$O_{P,e}^2$ at $\rho = 0.5$, 1.0 and 1.5 for $t_2 = 0.2$ is plotted for different values of U.

FIG. 18: (Color online) Edge density $\langle n_1^2 - n_L^2 \rangle$ for $t_1/t_2 = 0.3$ and 0.6 as function of the interaction strength ($L = 80$).

odd distances, however, one observes an interesting dependence of the parity order on the interaction strength, $O_{P,o} = -\frac{U}{\sqrt{16t_1^2 + U^2}}$. We plot the odd and even distance parity orders as $O_{P,e}$ and $O_{P,o}$ respectively with respect to U for different values of t_2 in Fig. 16. The black and red curves correspond to $O_{P,e}$ and $O_{P,e}$ respectively. The solid lines correspond to the limit of isolated double wells i.e for $t_2 = 0$. The dotted lines are the $t_2 = 0.2$ and the dashed curves are for $t_2 = 0.6$. It is very clear from this figure that the odd and even distance parities show two different behaviour and the parity order is finite in the MI, BO and PBO phases where as it is zero in the SF phase. Analogously one also finds for the gapped phases at half filling a finite oscillating parity order which is 0 for even and ± 1 for odd distances. The parity order parameter also vanishes in the SF phase. This can be seen from the Figure. 17 where $O_{P,e}^2$ is plotted as a function of U for different fillings.

V. TOPOLOGICAL PROPERTIES

A. Edge states

After having explored the bulk properties of the Model (1) we discuss the emergence of edge-states in this section. Recent study on bosonic SSH model shows that at half filling the gaped phases exhibit interesting nontrivial topological properties which have been discussed extensively by Grusdt et al. [16]. Due to the three-body constraint considered in the present work we may as well discuss topological properties of the unit filled system. The case of strong attractive interactions $-U \gg 1$ is dual to the hardcore boson limit $U \to \infty$ with renormalized hopping coefficients $t_i^{eff} = t_i^2/|U|$ at half filling. As effective on-site pairs are formed, one can define the corresponding operator $c_i^\dagger = (a_i^\dagger)^2|0\rangle$. The effective Hamil-
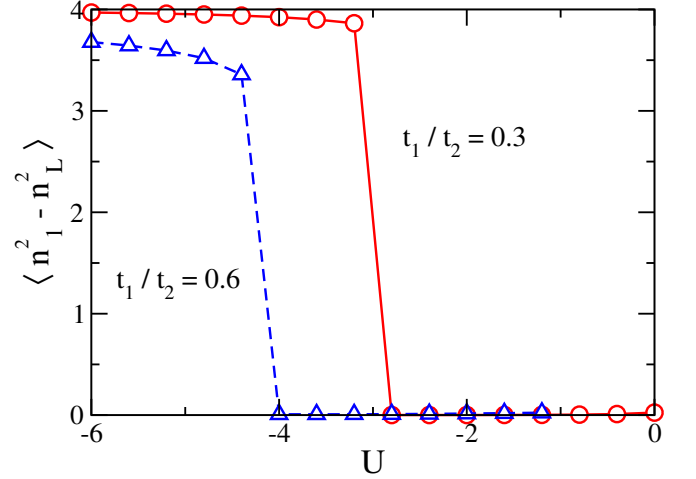
tonian for these pairs can be written as

$$\mathcal{H}_{eff} = -t_1^{eff} \sum_{i \, \in \, odd} (c_i^\dagger c_{i+1} + \text{H.c.})$$
$$-t_2^{eff} \sum_{i \, \in \, even} (c_i^\dagger c_{i+1} + \text{H.c.}) \qquad (9)$$

In this limit we may, hence, define a topological nontrivial winding number as defined in Eq. (10), or in a many-body context from the ground state ψ of the effective model with twisted boundary conditions $c_i \to e^{i\theta/L}c_i$,

$$\nu = i \int_0^{2\pi} d\theta \langle \psi(\theta)|\partial_\theta \psi(\theta)\rangle \qquad (10)$$

This allows to discriminate between the PBO_0 and a PBO_π region with $\nu = 0$ and $\nu = \pi$, respectively, for strong attractive interactions. Both regions are separated by a gapless PSF phase for the special point $t_2 = t_1$. For finite interactions the winding number is not exactly quantized and, thus, we observe a smooth crossover of both PBO_0 and PBO_π phases to the BO region without intermediate gapless phase.

The effective topological character of the PBO_π phase is reflected by the emergence of the edge states which is characterized from the edge density defined as $\langle n_1^2 - n_L^2 \rangle$ which, interestingly, can be observed for finite values of U. We plot this quantity for two different values of $t_1/t_2 = 0.3$ and $t_1/t_2 = 0.6$ with respect to U as shown in Fig. 18. In order to facilitate the numerical simulations we add a small symmetry breaking potential to the boundary sites of strength $\mu = 0.01t_2$. Comparisons to results with a smaller potential ($\mu = 0.001t_2$) and different system sizes (data not shown) indicate that our choice does not influence the physics of the system.

The point of emergence of edge states which is denoted as the blue cross-dot-dashed line differs from the BO-PBO crossover location in the phase diagram as depicted
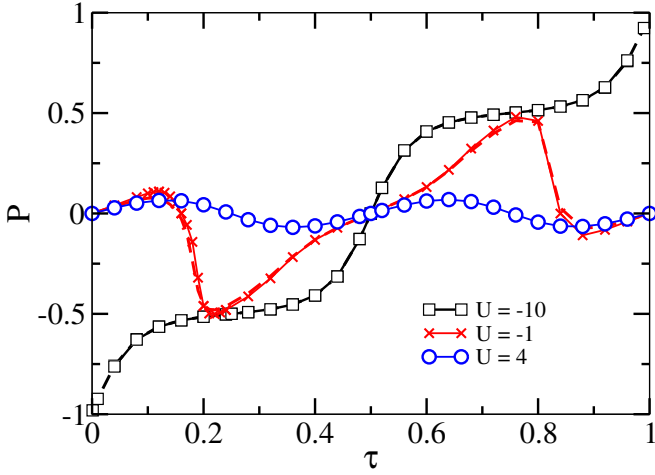
FIG. 19: (Color online) Polarization P for the RM model (11) as function of the adiabatic parameter τ for several values of U. Note that, $\tau = 0$ and 1 corresponds to $t_1 = 0.2$ and $t_2 = 1$ and for $\tau = 0.5$ we have $t_1 = 1.0$ and $t_2 = 0.2$. We consider system sizes of $L = 180$ sites and for comparison we show the $L = 80$ which is plotted as the dashed curve for $U = -1$. For $U = 4$ we plot $10 \times P$ for clarity.

in Fig. 12. The reason for this can be attributed to the bosonic enhancement which is energetically favourable to first delocalize a single doublon on the MI phase before the polarized edge states are formed [35].

B. Charge Pumping in the Rice-Mele model

The emergence of polarized edge states may be discussed more clearly in the framework of the Rice-Mele (RM)-like models [39], which smoothly connects the $t_2 < t_1$ and $t_1 < t_2$ half of the phase diagram of Fig. 12 by an additional parameter τ. We study this connection by the following Hamiltonian

$$\mathcal{H}_{RM} = -\sum_i (t - (-1)^i \delta t \cos(2\pi\tau)) a_i^\dagger a_{i+1} + \text{H.c.} +$$
$$+ \frac{\delta t}{2} \sin(2\pi\tau) \sum_i (-1)^i n_i + H_{int}. \quad (11)$$

where H_{int} contains the 2-body interaction term of Model (1). Here we choose $t = (t_1 + t_2)/2$ and $\delta t = (t_1 - t_2)/2$. Note, that now for $\tau = 0$ this corresponds to the $t_1 < t_2$ case of the SSH model Eq. (1) while the $t_2 < t_1$ case is realized for $\tau = 0.5$. A cycle of the τ-parameter can be interpreted as the realization of a Thouless-charge-pump [47], where a quantized charge or polarization is transported during an adiabatic time evolution.

In the single particle picture (i.e. for $U \to -\infty$) the pumped charge can be related to a Chern number of the RM model (defined on a torus in momentum k and τ space). Hence, here the pumped charge is quantized and
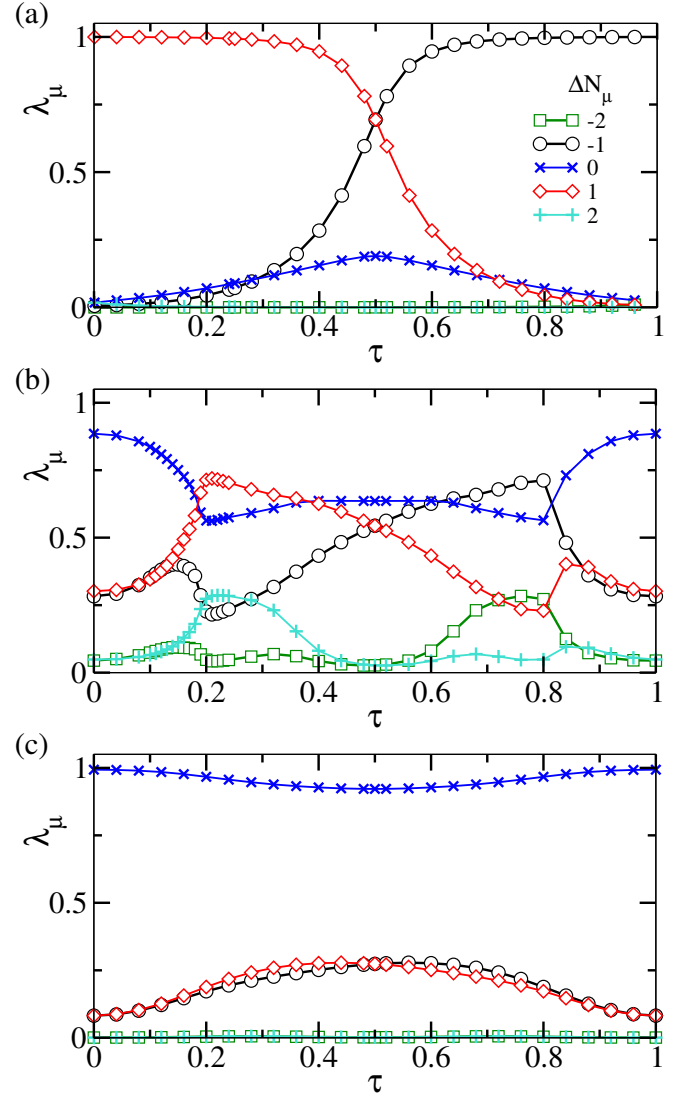

FIG. 20: (Color online) Largest values of the entanglement spectrum λ_μ of the reduced density matrix in the center of a finite system of size $L = 160$ for the RM model shown in Eq. (11) as a function of the adiabatic parameter τ for (a) $U = -10$, (b) $U = -1$ and (c) $U = 4$ (compare Ref. [21]). The eigenvalues λ_μ have been sorted by the particle number sector N_μ in the center of the chain and for convenience labeled by $\Delta N_\mu = N_\mu - L/2$.

directly linked to the non-trivial topology of the model if non-vanishing. Recently, with the observation of charge pumping in cold-atom experiments [17, 18], the fate of Thouless-pumping in interacting systems, such as the interacting fermionic or bosonic RM model has attracted a lot of interest [20, 21, 48]. Here we extend these ideas to the case of composite bosonic pairs at unit-filling, discussed in the previous sections.

Following Ref. [20] we study the charge pumping for finite systems with open-boundary conditions by moni-

toring the polarization

$$P(\tau) = \frac{1}{L} \sum_{i=0}^{L} \langle \psi(\tau) | (i - i_0) n_i | \psi(\tau) \rangle \qquad (12)$$

with $i_0 = (L - 1)/2$ and the ground state $\psi(\tau)$ of Model (11). The total transferred charge is given by

$$Q = \int_0^1 d\tau \partial_\tau P(\tau) \qquad (13)$$

and, hence, directly linked to the presence of polarized edge state for the SSH-model. We plot the polarization over the pump-cycle in Fig. 19 for several values of the interactions. In our calculation we consider when $\tau = 0$ or 1, the value of $t_1 = 0.2$ and $t_2 = 1$ and vice-versa when $\tau = 0.5$. While for strong attractive interactions $U = -10$ we observe a clear pumping of a charge $Q = 2$ corresponding to a bosonic pair, for $U = -1$ and $U = 4$ we find zero pumped charge i.e. $Q = 0$, corresponding to the abrupt vanishing of polarized edge states discussed in the previous section. Remarkably, we cannot link the breakdown of the charge-pumping to a gap-closing in the pumping cycles shown in Fig. 19.

As discussed recently by Hayward et al. [21] the charge-pumping in the RM model may as well be visualized by the evolution of the entanglement spectrum λ_μ. In Fig. 20 we plot the largest eigenvalues λ_μ of the reduced density matrix in the center of the system. Due to the total particle number conservation of the model the eigenvalues may be labeled by $\Delta N_\mu = N_\mu - N_0$, where N_μ corresponds to the quantum number of the eigenvalues λ_μ and $N_0 = N/2$. With this we may calculate the polarization using [21, 49]

$$P = \sum_\mu \Delta N_\mu \lambda_\mu^2 . \qquad (14)$$

As shown in Fig. 20 for strong attractive interaction $U = -10$, the $\Delta N_\mu = \pm 1$ eigenstates dominate, leading to a non-zero pumped charge. With increasing U we observe a smooth crossover to the MI regime where the $\Delta N_\mu = 0$ state has the largest contribution and no charge is pumped.

VI.   CONCLUSIONS

We investigate the ground state properties of a system of three-body constrained bosons in a SSH type model.

By analysing the competition between the dimerized hopping and onsite interaction we obtain the complete phase diagram both in the regime of attractive as well as repulsive interactions. The possibility of two types of hopping dimerization leads to distinguished bulk and edge physics. In the bulk both the hopping dimerization stabilizes various gapped BO and MI phases at commensurate densities. At unit filling and small hopping ratios the system exhibits a BO phase of pairs which we call the PBO phase and there exists smooth crossover from MI-BO(BO-PBO) on the repulsive(attractive) side of the phase diagram. For large values of the hopping ratios, the gapped phases melt for small values of interactions and there exist an intermediate SF phase. The appropriate finite size scaling show that the superfluid to gapped phase transitions are of BKT type. The PBO phase, a bond-order phase of hardcore pairs, exists for both the dimerization at large values of attractive interactions. These PBO phases possess two distinct winding number ν and for $\nu = \pi$, being linked to interesting edge states. To further analyse the emergence of edge states in the case of composite boson pairs we analyse the phenomena of Thouless-charge pumping in the context of Rice-Mele model which can be generalized to the SSH model at unit filling. The various phases are characterized by computing the corresponding order parameters which are of experimental relevance. At incommensurate densities and for large attractive interactions the bosons paired up to form the PSF phase.

The findings presented in this work addresses an interesting problem which involves the physics of strongly correlated bosons in a topological model. The emergence of edge states in the topological PBO phases may attract further interest to understand the properties of bound states. The current prediction can in principle be experimentally accessible with the existing state-of-the art ultracold atom experiment along the line of recent experiment on Rydberg atoms in SSH model [15].

[1] M. Greiner, O. Mandel, T. Esslinger, T. W. Hänsch, and I. Bloch, Nature **415**, 39 (2002).

[2] D. Jaksch, C. Bruder, J. I. Cirac, C. W. Gardiner, and P. Zoller, Phys. Rev. Lett. **81**, 3108 (1998).

[3] M. Lewenstein, A. Sanpera, and V. Ahufinger, Contemporary Physics **54** (2013).

[4] I. B. Spielman, W. D. Phillips, and J. V. Porto, Phys. Rev. Lett. **98**, 080404 (2007).

[5] D. van Oosten, P. van der Straten, and H. T. C. Stoof, Phys. Rev. A **63**, 053601 (2001).

[6] I. Danshita, J. E. Williams, C. A. R. Sá de Melo, and C. W. Clark, Phys. Rev. A **76**, 043606 (2007).

[7] G. Vidal, Phys. Rev. Lett. **93**, 040502 (2004).

[8] J. Sebby-Strabley, M. Anderlini, P. S. Jessen, and J. V. Porto, Phys. Rev. A **73**, 033605 (2006).

[9] J. Sebby-Strabley, B. L. Brown, M. Anderlini, P. J. Lee, W. D. Phillips, J. V. Porto, and P. R. Johnson, Phys. Rev. Lett. **98**, 200405 (2007).

[10] W. P. Su, J. R. Schrieffer, and A. J. Heeger, Phys. Rev. Lett. **42**, 1698 (1979).

[11] S. Ryu and Y. Hatsugai, Phys. Rev. Lett. **89**, 077002 (2002).

[12] P. Delplace, D. Ullmo, and G. Montambaux, Phys. Rev. B **84**, 195452 (2011).

[13] L.-J. Lang, X. Cai, and S. Chen, Phys. Rev. Lett. **108**, 220401 (2012).

[14] M. Atala, M. Aidelsburger, J. T. Barreiro, D. Abanin, T. Kitagawa, E. Demler, and I. Bloch, Nature Physics **9**, 795 (2013).

[15] S. de Léséleuc, V. Lienhard, P. Scholl, D. Barredo, S. Weber, N. Lang, H. P. Büchler, T. Lahaye, and A. Browaeys, ArXiv e-prints (2018), 1810.13286.

[16] F. Grusdt, M. Höning, and M. Fleischhauer, Phys. Rev. Lett. **110**, 260405 (2013).

[17] M. Lohse, C. Schweizer, O. Zilberberg, M. Aidelsburger, and I. Bloch, Nature Physics **12**, 350 (2015).

[18] S. Nakajima, T. Tomita, S. Taie, T. Ichinose, H. Ozawa, L. Wang, M. Troyer, and Y. Takahashi, Nature Physics **12**, 296 (2016).

[19] Y. E. Kraus, Y. Lahini, Z. Ringel, M. Verbin, and O. Zilberberg, Phys. Rev. Lett. **109**, 106402 (2012).

[20] M. Nakagawa, T. Yoshida, R. Peters, and N. Kawakami, arXiv preprint arXiv:1802.09780 (2018).

[21] A. Hayward, C. Schweizer, M. Lohse, M. Aidelsburger, and F. Heidrich-Meisner, arXiv preprint arXiv:1810.07043 (2018).

[22] S. Will, T. Best, U. Schneider, L. Hackermüller, D.-S. Lühmann, and I. Bloch, Nature **465**, 197 (2010).

[23] D. S. Petrov, Phys. Rev. Lett. **112**, 103201 (2014).

[24] D. S. Petrov, Phys. Rev. A **90**, 021601 (2014).

[25] P. R. Johnson, E. Tiesinga, J. V. Porto, and C. J. Williams, New Journal of Physics **11**, 093022 (2009).

[26] A. J. Daley, J. M. Taylor, S. Diehl, M. Baranov, and P. Zoller, Phys. Rev. Lett. **102**, 040402 (2009).

[27] A. Safavi-Naini, J. von Stecher, B. Capogrosso-Sansone, and S. T. Rittenhouse, Phys. Rev. Lett. **109**, 135302 (2012).

[28] A. J. Daley, J. M. Taylor, S. Diehl, M. Baranov, and P. Zoller, Phys. Rev. Lett. **102**, 040402 (2009).

[29] L. Bonnes and S. Wessel, Phys. Rev. Lett. **106**, 185302 (2011).

[30] B.-l. Chen, X.-b. Huang, S.-p. Kou, and Y. Zhang, Phys. Rev. A **78**, 043603 (2008).

[31] T. Sowiński, R. W. Chhajlany, O. Dutta, L. Tagliacozzo, and M. Lewenstein, Phys. Rev. A **92**, 043615 (2015).

[32] M. Singh, T. Mishra, R. V. Pai, and B. P. Das, Phys. Rev. A **90**, 013625 (2014).

[33] M. Singh, S. Mondal, B. K. Sahoo, and T. Mishra, Phys. Rev. A **96**, 053604 (2017).

[34] S. Greschner, L. Santos, and T. Vekua, Phys. Rev. A **87**, 033609 (2013).

[35] M. Di Liberto, A. Recati, I. Carusotto, and C. Menotti, The European Physical Journal Special Topics **226**, 2751 (2017), ISSN 1951-6401.

[36] J. Zak, Phys. Rev. Lett. **62**, 2747 (1989).

[37] P. Delplace, D. Ullmo, and G. Montambaux, Phys. Rev. B **84**, 195452 (2011).

[38] L.-J. Lang, X. Cai, and S. Chen, Phys. Rev. Lett. **108**, 220401 (2012).

[39] M. Rice and E. Mele, Phys. Rev. Lett. **49**, 1455 (1982).

[40] M. Singh, A. Dhar, T. Mishra, R. V. Pai, and B. P. Das, Phys. Rev. A **85**, 051604 (2012).

[41] A. Dhar, M. Maji, T. Mishra, R. V. Pai, S. Mukerjee, and A. Paramekanti, Phys. Rev. A **85**, 041602 (2012).

[42] S.-J. Gu, Int. J. Mod. Phys. B **24**, 4371 (2010).

[43] T. Mishra, J. Carrasquilla, and M. Rigol, Phys. Rev. B **84**, 115135 (2011).

[44] M. Dalmonte, J. Carrasquilla, L. Taddia, E. Ercolessi, and M. Rigol, Phys. Rev. B **91**, 165136 (2015).

[45] W. S. Bakr, J. I. Gillen, A. Peng, S. Fölling, and M. Greiner, Nature **462**, 74 (2009).

[46] J. F. Sherson, C. Weitenberg, M. Endres, M. Cheneau, I. Bloch, and S. Kuhr, Nature **467**, 68 (2010).

[47] D. Thouless, Phys. Rev. B **27**, 6083 (1983).

[48] E. Berg, M. Levin, and E. Altman, Phys. Rev. Lett. **106**, 110405 (2011).

[49] M. P. Zaletel, R. S. K. Mong, and F. Pollmann, Journal of Statistical Mechanics: Theory and Experiment **2014**, P10007 (2014).